The Central United States Seismic Observatory: Site Characterization, Instrumentation, and Recordings

by Edward W. Woolery, Zhenming Wang, N. Seth Carpenter, Ron Street, and Clayton Brengman

ABSTRACT

The Central United States Seismic Observatory is a vertical seismic array located in southwestern Kentucky within the New Madrid seismic zone. It is intended to describe the effects of local geology, including thick sediment overburden, on seismic-wave propagation, particularly strong motion. The three-borehole array is composed of seismic sensors placed on the surface, in the bedrock, and at various depths within the 585-m-thick sediment overburden. The array's deep borehole also provided a unique opportunity in the northern Mississippi embayment for the direct geologic description and geophysical measurement of the complete Late Cretaceous–Quaternary sediment column. A seven-layer intrasediment velocity model is interpreted from the complex, inhomogeneous stratigraphy. The *S*- and *P*-wave sediment velocities range between 160 and 875 m/s and between 1000 and 2300 m/s, respectively, and their bedrock velocities range between 1452 and 3775 m/s, respectively. Seismometers and accelerometers operate both at the surface and 2 m into bedrock, with strong-motion accelerometers at depths of 30, 259, and 526 m. The array operation has been frequently interrupted by the large hydrostatic pressures on the deeper instrumentation; however, the full array has recorded weak-motion response from 95 earthquakes at local, regional, and teleseismic distances. Initial observations reveal a complex spectral mix of amplification and de-amplification across the array, indicating the site effect in this deep-sediment setting is not simply generated by the shallowest layers. Preliminary horizontal-to-vertical spectral ratio (H/V) experiments show the bedrock vertical and horizontal amplitudes are not equal, a required assumption for site characterization. Further, there are marked differences between spectral ratios from the directly measured transfer function (H/H) and H/V for particular earthquakes. On average, however, the H/H and H/V methods are coincident within a narrow band of frequencies ranging between 0.35 and 1.1 Hz.

INTRODUCTION

Observations from Mexico City during the 19 September 1985, Michoacán earthquake (Seed *et al.*, 1988) and the San Francisco Marina District during the Loma Prieta earthquake of 18 October 1989 (Bonilla, 1991) provided clear and well-documented evidence that local geology, including thick soil/sediment overburden, can alter the amplitude, frequency content, and duration of earthquake ground motions. Numerous dynamic and geometric properties are responsible for these ground-motion variation effects, including media elasticity, impedance contrasts within the sediment overburden and at the sediment–bedrock interface, sediment thickness, surface topography, sediment–bedrock interface geometry (i.e., horizontal, irregular, dipping, etc.), ground-motion amplitude (i.e., linear versus nonlinear), and the existence of lateral and/or vertical velocity gradients in the sediment and/or bedrock. Therefore, an earthquake's resultant ground motions consist of a complex mixture of source, path, and site effects, including 3D effects (e.g., Bard and Chavez-Garcia, 1993; Anderson *et al.*, 1996; among others).

Simplified-empirical, pseudotheoretical, reference-site, and vertical-array methods are field-based measures often used for characterizing site effects; however, there is considerable uncertainty associated with each due to the inability to constrain the complex causality, particularly in regions with deep basins containing inhomogeneous sediment deposits (> 100 m) such as the central United States (Steidl *et al.*, 1996; Bommer and Abrahamson, 2006). The simplified-empirical method considers two parameters for characterizing the site effect: the incoming bedrock ground motion and time-weighted average shear-wave velocity for the top 30 m (V_{S30}) of earth material (Building Seismic Safety Council, 2009). Generally stated, the site coefficient increases with decreasing V_{S30}. In the Los Angeles area, Wald and Mori (2000) found simplified empirical characterizations based on V_{S30} approximated the site response observations, but the scatter was large and inadequate for site amplification prediction. Castellaro *et al.* (2008) stated site amplification is too complex to be characterized simply by V_{S30}. Conversely, Molnar *et al.* (2004) concluded that site response based on V_{S30} in the greater Victoria, British Columbia, area is in agreement with the intensities observed for the 2001 Nisqually earthquake in Washington state. Alternatively, the horizontal-to-vertical (H/V) spectral ratio is another widely used cost-effective method for estimating the site effect (Nakamura,

doi: 10.1785/0220150169

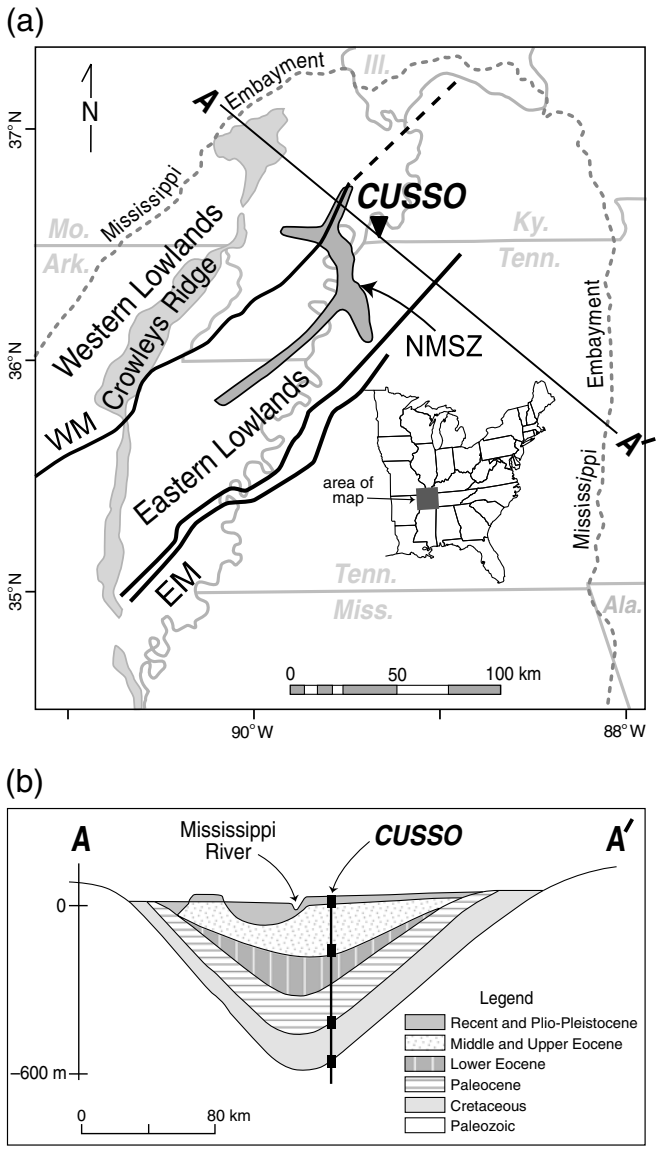

▲ **Figure 1.** (a) The seismotectonic and physiographic setting. The Central United States Seismic Observatory (CUSSO) is located ~12 km northeast of the northwest-trending central stepover arm of the New Madrid seismic zone (NMSZ) (dark gray shaded area). The NMSZ is located primarily in the Reelfoot rift (heavy black lines) (modified from Csontos and Van Arsdale, 2008). The structure of the Reelfoot rift area is overlain by the Mississippi embayment sediments. (b) A–A′ cross section of the embayment shows the relative location of CUSSO within the sediment overburden and central embayment axis (modified from Toro *et al.*, 1992).

1989). This pseudotheoretical approach can include using the horizontal-to-vertical spectral ratio of ambient-noise/microtremor (e.g., Bodin and Horton, 1999; Castellaro and Mulargia, 2009; among others), or the horizontal-to-vertical spectral ratio of the energetic part of earthquake *S* waves (e.g., Lermo and Chavez-Garcia, 1993; Castro *et al.*, 1997; Chen and Atkinson, 2002; among others). Both approaches assume that the vertical component of the ground motions is relatively uninfluenced by the geologic site conditions and the effects of Rayleigh waves on the horizontal and vertical components are equivalent; thus, the resultant horizontal-to-vertical spectral ratio ideally removes the source and path effects of the noise, leaving only the site response signal (Castro *et al.*, 1997; Bonnefoy-Claudet *et al.*, 2006). A more direct and reliable way for separating an earthquake's source and path effects from the site effect is to simultaneously record the earthquake on rock and the ground surface. This can be performed in two ways: (1) a comparison of free-field ground motions at one or more locations with a reference recording from a nearby rock site (Steidl *et al.*, 1996) or (2) using a vertical array of downhole (i.e., bedrock) and surface instruments (Archuleta *et al.*, 1992; Field *et al.*, 1998) and simultaneously recording ground motions at a site.

To use the latter direct method for deep sedimentary site-effect characterization in the northern Mississippi embayment of the central United States, a three-borehole, 21-component vertical seismic array, called the Central United States Seismic Observatory (CUSSO), was installed near the most active part of the New Madrid seismic zone (NMSZ) (Figs. 1 and 2). The deepest borehole penetrates 585 m of unlithified Mississippi embayment sediment and into the underlying bedrock; it is among the deepest conventional continental vertical seismic arrays in operation. Basic goals for the array include (1) observational evidence of deep sediment/soil effects on strong- and weak-motion amplification and attenuation of seismically induced ground motions, including frequency and duration modulation, and (2) a calibration and reference measure for regional free-field strong-motion and seismic installations. Although the full array has experienced frequent operational interruptions since its initial installation in September 2009, it successfully recorded several earthquakes on all components between autumn 2009 and spring 2011. During this period of time, the bedrock accelerometer was operational and earthquakes were recorded at local, regional, and teleseismic distances, including the stronger earthquakes from the 2010–2011 Arkansas swarm (Horton, 2012).

SITE LOCATION AND SEISMIC SETTING

Geographically, CUSSO is located in a small rural community situated atop a subtle topographic high (~3 m), called Sassafras Ridge, within the Mississippi River floodplain of westernmost Kentucky (Fig. 1). The site coordinates are N36°33.139′, W89°19.784′, and the location is typical of what Toro *et al.* (1992) referred to as embayment lowlands (i.e., floodplains) that cover much of the northern Mississippi embayment region of western Kentucky, southeastern Missouri, northwestern Tennessee, and northeastern Arkansas. Two important parts of the CUSSO location criteria included proximity to an area of high seismicity in order to maximize the number of recorded events in the shortest amount of time and site conditions typical of those found throughout the region and at most free-field regional seismic network stations.

The NMSZ is an intraplate area of relatively high seismic energy release and includes a historic sequence of at least three large earthquakes ($\mathbf{M} > 7$) that occurred during the winter of

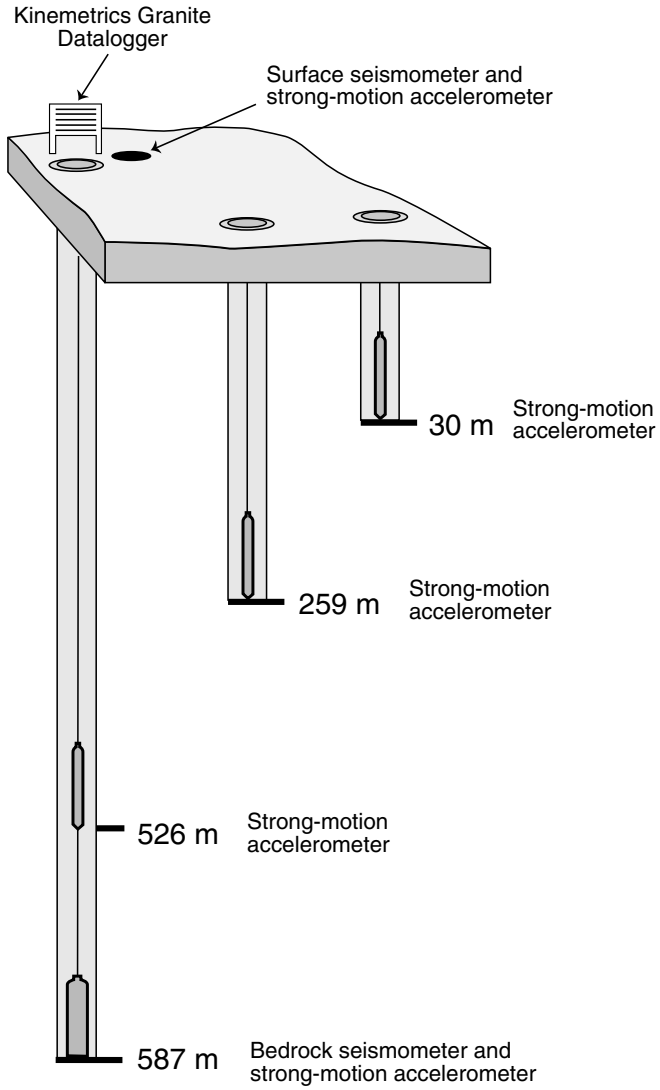

▲ **Figure 2.** The three-borehole CUSSO array, including the instrumentation and depth below ground surface. The 587 m instrumented well is laterally separated from the 259 and 30 m wells by 23.5 and 25.5 m, respectively. The 259 and 30 m wells are separated by 7.1 m. The free-surface instrumentation is offset from the 595 m wellhead by 3.5 m.

1811–1812, as well as similar clustered events found in the paleoseismic record (Johnston and Schweig, 1996; Tuttle *et al.*, 2002) (Fig. 1). These historic and paleoseismic events make the NMSZ a primary contributor to the seismic hazard for much of the central United States. Most of the contemporary seismicity lies within the early Paleozoic Reelfoot rift system and beneath the Late Cretaceous and early Tertiary Mississippi embayment, an elongate southwest-plunging sediment-filled basin that merges with the Gulf of Mexico coastal plain (Van Arsdale and TenBrink, 2000; Cox and Van Arsdale, 2002; Csontos and Van Arsdale, 2008). The earthquake epicenter patterns and associated focal solutions allow the complex NMSZ to be generalized as two northeast-oriented dextral strike-slip fault zone segments offset by a central northwest-oriented left-stepping restraining-bend thrust. CUSSO is sited 12 km northeast of the most seismically active part of the zone, the central stepover arm, and near the central axis of the Mississippi embayment (Fig. 1).

SITE STRATIGRAPHY

The Paleozoic bedrock was reached in the deepest of CUSSO's three boreholes, at 1920 ft (585 m) below ground surface. We provide a relatively detailed description of the numerous unlithified post-Paleozoic sediment deposits, because few places exist in the northern Mississippi embayment where the stratigraphic sequence for this overburden can be directly observed. Although retrieving *in situ* cored sediment samples was cost prohibitive, we were able to establish stratigraphic boundaries from visual analysis of collected well-head "cuttings" compared with a suite of downhole petrophysical logs performed by GeoVision Inc. (i.e., natural gamma ray [NGAM], resistivity, and *P*/*S* sonic velocity) (Figs. 3 and 4). Cuttings represent a mixture of the sediment being drilled through at certain intervals of depth, including from higher in the borehole; therefore, cuttings cannot be used to describe intraformation features such as bedding or the nature of the formation contacts, but, in the absence of core, they provide useful information on general rock/sediment type and mineralogy at depth, which can be compared with geophysical logs to interpret subsurface stratigraphy.

Quaternary Alluvium (Pleistocene–Recent)

The alluvium cover in the CUSSO borehole is 157 ft (48 m) thick, and consists mostly of fine to coarse sands. Regionally, there is a substantial unconformity between Quaternary alluvium and the underlying sediments in the region (Olive, 1980; McDowell *et al.*, 1981). The contact between Quaternary sediments and the underlying Jackson formation is interpreted in the CUSSO hole at the base of coarse sands and gravel, as well as a marked change in the NGAM curve at 157 ft (48 m) (Fig. 3). Finch (1971) also indicates that gravels typically occur at base of the alluvium and at the base of older continental deposits above the Jackson formation in the area.

Jackson Formation (and Possibly Upper Claiborne?) (Oligocene?–Eocene)

The Jackson formation is an unlithified silty clay with a few interbedded silts and sands (Finch, 1971; Olive, 1980). Unfortunately, Jackson clays, silts, and sands are similar to the underlying Claiborne formation, making visual distinction difficult. In the nearby Florence No. 1 Smith well, Davis *et al.* (1973) could not differentiate the Jackson from underlying upper Claiborne and correlated the combined Jackson through upper Claiborne interval as a single, undifferentiated unit. In the CUSSO well, the top of the Jackson formation is placed at the base of a gravel and the top of a black clay. The base of the unit is placed at the base of a sand overlying a sandy clay at 430 ft (131 m) that also exhibits a distinct change in the NGAM and resistivity log response (Fig. 3). Davis *et al.* (1973) placed the base of the combined Jackson–upper Claiborne interval at a level that could be correlated to the base of the

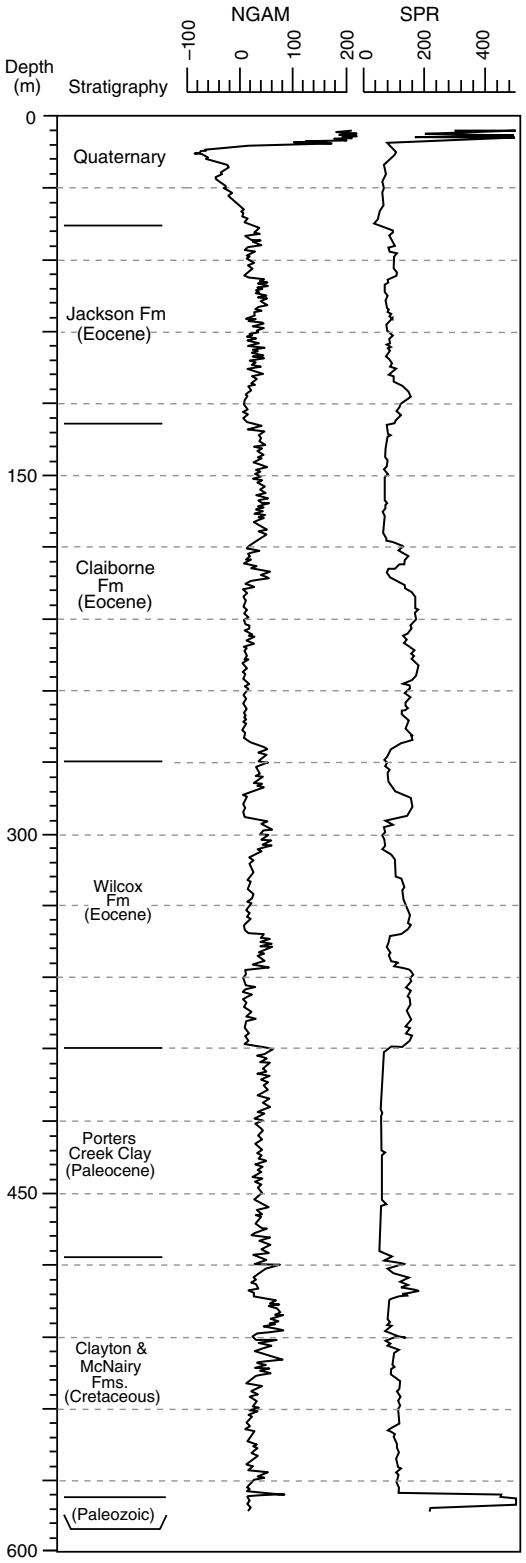

▲ **Figure 3.** Wireline log of the deeded CUSSO borehole. The CUSSO site consists of 585 m of unlithified sediment overlying the carbonate Paleozoic bedrock. The stratigraphic interpretation for the sediment was derived from the logged borehole cuttings during the drilling process, as well as natural gamma ray and electrical resistivity logs in the completed hole. NGAM, natural gamma ray (counts/s); SPR, single-point resistivity (Ω · m).

Jackson as picked in the CUSSO well or possibly to a clay higher in the hole.

Claiborne Group (Lower–Middle Eocene)

Regionally, the contact between the Jackson and Claiborne formations is conformable (Olive, 1980). The Claiborne is composed of sands, silts, and clays. Silts and clays can contain carbonaceous material, as well as occasional lignite beds (Nelson, 1998). In ascending order, the Claiborne is separated into the Carrizo sand, Cane River formation, Sparta sand, Cook Mountain formation, and Cockfield formation (the Carrizo and Sparta comprise the Memphis sand in Tennessee) but thins northward in the Mississippi embayment into Kentucky, where it is undifferentiated. In the CUSSO well, the base of the Claiborne is picked at the base of a dense or cemented sand at 880 ft (268 m) depth, which also shows sharp changes in the NGAM and resistivity logs (Fig. 3). This is similar to the base of the Claiborne picked in the nearby Florence No. 1 Smith well by Davis *et al.* (1973).

Wilcox Formation (Upper Paleocene–Lower Eocene)

The Wilcox formation consists of sands, silts, clays, and gravels with some lignite at various locations. Sands are fine to very fine grained; clays are often sandy and silty, with occasional carbonaceous inclusions. Regionally, the top and bottom of the Wilcox formation are unconformable. In the CUSSO well, the top of the Wilcox formation is picked beneath the dense or cemented sand at approximately 268 m, and the base is picked at the top of a hard, thick, black silty clay at 396 m, showing sharp changes in NGAM and resistivity responses on the wireline log (Fig. 3).

Porters Creek Clay (Early Paleocene)

Below the Wilcox, the Midway group consists of the Porters Creek clay, which lies unconformably below the Wilcox formation and is composed of hard clay with glauconitic sands common in its upper and lower parts (Olive, 1980). In the CUSSO well, the top of the Porters Creek clay is picked in the driller's log at the top of a described hard black indurated clay at approximately 396 m depth, which is a distinctive lithology for the unit. This contact exhibits strong changes in the wireline logs. The base of the Porters Creek clay is picked at the base of a sequence of clay-dominant sediment on the geophysical logs just above a sandy clay at approximately 488 m depth (Fig. 3). This is similar to the top and base picked by Davis *et al.*, (1973) in the nearby Florence No. 1 Smith well, and, for reasons of practicality, separates the thick clay interval from underlying mixed clays, silts, and sand. Regionally, the underlying Clayton formation contains similar clays, silts, and sands to those that can occur in the Porters Creek formation, so the contact should be considered approximate. Palynological analyses would be needed to confirm the boundary.

Clayton–McNairy Formations (Late Cretaceous)

The undifferentiated Clayton–McNairy formation is a loose to friable micaceous sand with interbedded clays and silts. Sands in the Clayton and McNairy are lithologically indistinguishable

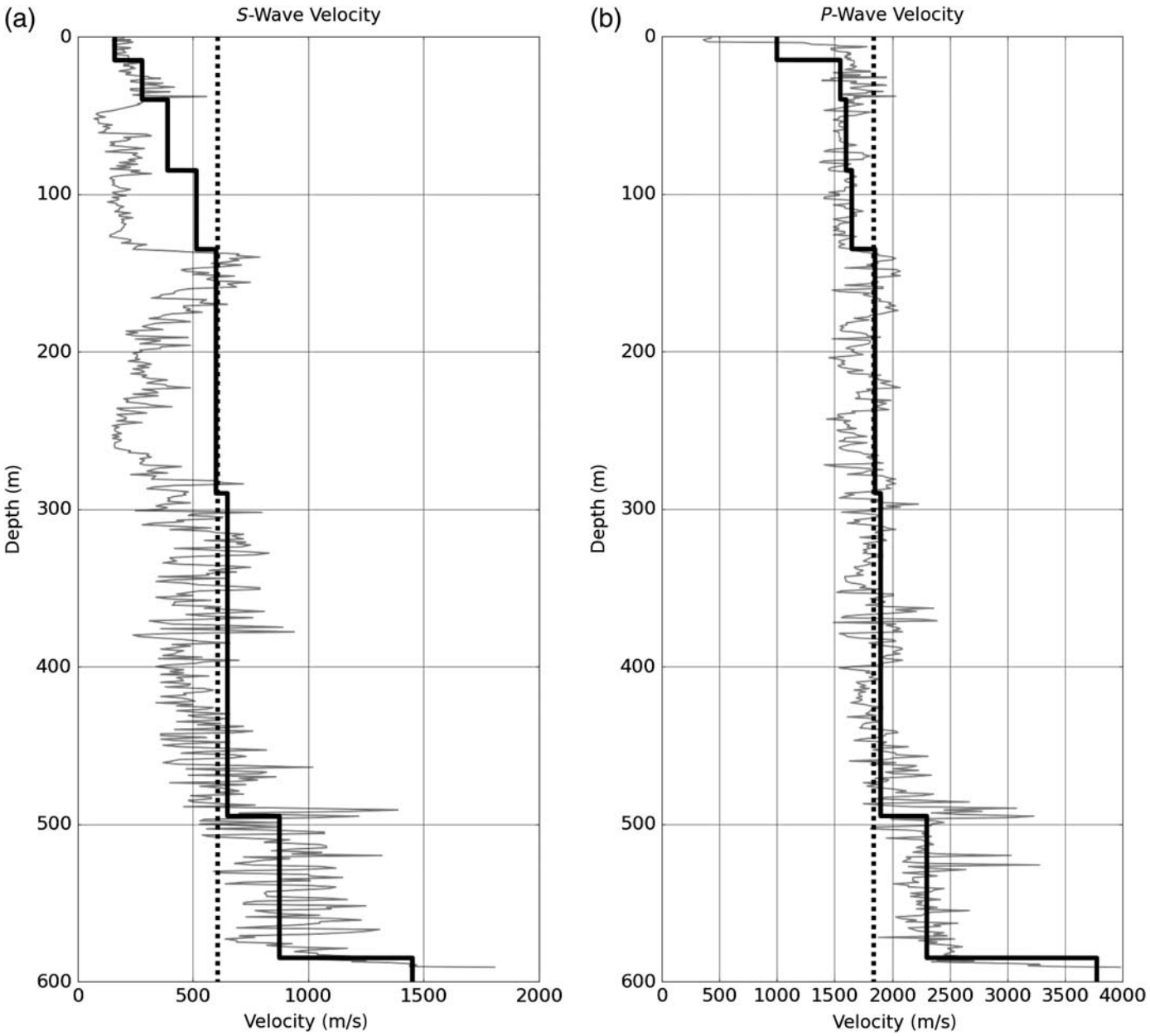

▲ **Figure 4.** (a) The defined *S*-wave and (b) *P*-wave velocity models are shown by the solid black lines. These are compared with the *S*- and *P*-wave suspension velocity logs (gray solid line) and the average sediment velocity as measured by the phase arrival times across the instrumented array (vertical broken gray line) from the deepest CUSSO borehole. Two zones of anomalously low velocity are exhibited in the depth intervals of 50–130 and 180–265 m in both the *P*- and *S*-wave suspension logs but are more pronounced in the *S*-wave log. We interpret the anomalies as artifacts created in the immediate vicinity of the borehole by the drilling process. Specifically, considerable borehole wall instability and collapse were noted during the drilling of these depth intervals; consequently, we speculate that the substantial sediment disturbance in the borehole annulus and immediate vicinity altered the velocity suspension log measurements.

so have been commonly mapped together in the region (e.g., Finch, 1971). At the CUSSO site, the undifferentiated Clayton–McNairy formation extends from the top of hard sandy clay at approximately 488 m depth to the bedrock unconformity at 585 m, where resistivity increases sharply (Fig. 3). This is similar to the correlation of undifferentiated Clayton–McNairy formation in the Florence No. 1 Smith well by Davis *et al.* (1973).

Paleozoic Bedrock

Bedrock was reached at 585 m depth in the well. Fragments of rock noted at the top of rock likely represent rubble associated with significant bedrock weathering at this major unconformity. The borehole was advanced to 595 m in the underlying carbonates, but drilling fluid loss, possibly associated with karst or open fractures, terminated the borehole prior to reaching its planned 30-m-bedrock-penetration depth. The top of the

Paleozoic bedrock at the CUSSO site is part of the upper Ordovician Knox supergroup based on regional mapping (Potter and Pryor, 1961; Schwalb, 1969).

SITE VELOCITY MODEL

The seismic velocity model at the site, shown in Figure 4, is composed of seven layers over a bedrock half-space (Brengman, 2014). The model was constructed from three primary sources: (1) surface seismic reflection and refraction surveys; (2) *P*- and *S*-wave suspension velocity logs by Geovision, Inc., of the total 595 m borehole depth; and (3) measured phase arrival times across the instrumented array. Woolery and Wang (2010) reported *P*- and *S*-wave velocity measurements made from downhole velocity suspension logs and surface seismic walkaway soundings. In addition, earthquake phase arrival observations between the surface and bedrock instruments provided bulk average *S*- and *P*-wave velocity measurements of 610 and 1836 m/s, respectively, for the sediment column. They also noted low-velocity inconsistencies between results of the suspension logs and the seismic walkaway soundings. Two zones of anomalously low velocity are exhibited in the depth intervals of 50–130 and 180–265 m below ground surface in both the *P*- and *S*-wave suspension logs but are more pronounced in the *S*-wave log.

Although the suspension logs are not susceptible to blind zones and provide a higher-resolution velocity measure relative to the surface soundings, the two low-velocity zones manifested in the suspension logs are interpreted as artifacts created in the immediate vicinity of the borehole by the drilling process. Specifically, considerable borehole wall instability and collapse were noted during the drilling of these depth intervals; consequently, we speculate that the substantial sediment disturbance in the borehole annulus and immediate vicinity altered the velocity suspension log measurements and produced results not indicative of true *in situ* conditions immediately following borehole completion.

The average *P*- and *S*-wave velocity values measured from the phase observations are also similar to the average velocities found from the refraction and reflection walkaway sounding measurements (Woolery and Wang, 2010). We interpret the average *S*-wave velocity to be approximately 300 m/s higher than the weighted average predicted by the suspension log measurements. This also suggests that the suspension velocity measurements are anomalous and perhaps caused by sediment disturbance localized around the borehole. The seven layers that make up the velocity profile correlate well with observed stratigraphic horizons: the lower boundary of layer 1 correlates with the top of the basal Quaternary gravel, and the lower boundaries of layers 2, 4, 5, 6, and 7 are at the interpreted basal boundaries for the Jackson, Claiborne, Wilcox, Porters Creek clay, and Clayton–McNairy formations, respectively.

In addition to the intricate unlithified sediment stratigraphy, other aspects of the CUSSO geologic site model are equally complex. Woolery and Almayahi (2014) showed a series of high-resolution *P*-wave seismic-reflection surveys in a 1-km-radius surrounding CUSSO that imaged steeply dipping N30° E striking faults that uplifted and arched post-Paleozoic sediments in a manner consistent with a dextral strike-slip component of displacement. They traced subparallel faults beneath the array, and the images show the deformation extends above Paleozoic bedrock, affecting the Late Cretaceous and Eocene Mississippi embayment sediments, as well as the base of the Quaternary. The Paleozoic and Cretaceous horizons have as much as 75 and 50 m of relief, respectively, with the middle Eocene and basal Quaternary disrupted 25 and 15 m, respectively.

ARRAY CONFIGURATION, INSTRUMENTATION, AND OPERATION

Configuration

CUSSO is a 21-component vertical seismic array with sensors deployed at various elevations between the surface and bedrock (Fig. 2). The subsurface instruments reside in three adjacent boreholes drilled to depths of 30, 259, and 595 m. These vertical arms were constructed and instrumented in two phases: the first included drilling and installation of the 30 and 259 m wells during the fall of 2006, and the second was for the deep 595 m well during the fall of 2009. The intermediate and deep vertical arms hold accelerometers and a seismometer at major impedance boundaries identified in the site characterization surveys, whereas the shallow 30 m borehole, housing an accelerometer, was specifically placed to correspond with the empirically defined dynamic site-coefficient boundary given by the Building Seismic Safety Council (2009); thus, its shallow depth is configured to evaluate the applicability of the current National Earthquake Hazards Reduction Program (NEHRP) ground-motion scaling factors that are derived from the time-averaged shear-wave velocity of the uppermost 30 m of strata. This borehole was auger drilled and completed with 102-mm-diameter schedule 40 PVC casing and a tremie cement–bentonite backfill.

The 259 m intermediate arm of the array was instrumented with an accelerometer. This elevation was selected based on a strong impedance boundary identified in seismic-reflection walkaway soundings and common-midpoint profiles (Woolery and Wang, 2010, 2012; Woolery and Almayahi, 2014). Stratigraphically, this correlates with the base of the Memphis sand, a lower unit of the Claiborne group (Fig. 3). The borehole was drilled using a mud-rotary method and completed with 102 mm steel casing and a tremie cement–bentonite backfill.

The deep borehole was advanced using a telescoped mud-rotary operation. An initial 38-cm-diameter borehole was drilled and cased to a depth of 46 m below the surface to stabilize the loose alluvium. The second part of drilling advanced a 25-cm-diameter boring through the remaining sediment. The total sediment thickness at the site was 585 m. The borehole was terminated at a final depth of 595 m (~10 m into rock). The drilling encountered considerable side-wall instability problems throughout the top 260 m, likely altering *in situ* conditions in the neighborhood of the borehole annulus and effecting suspension velocity measurements. An accelerometer and seismometer were installed 2 m beneath the sediment–

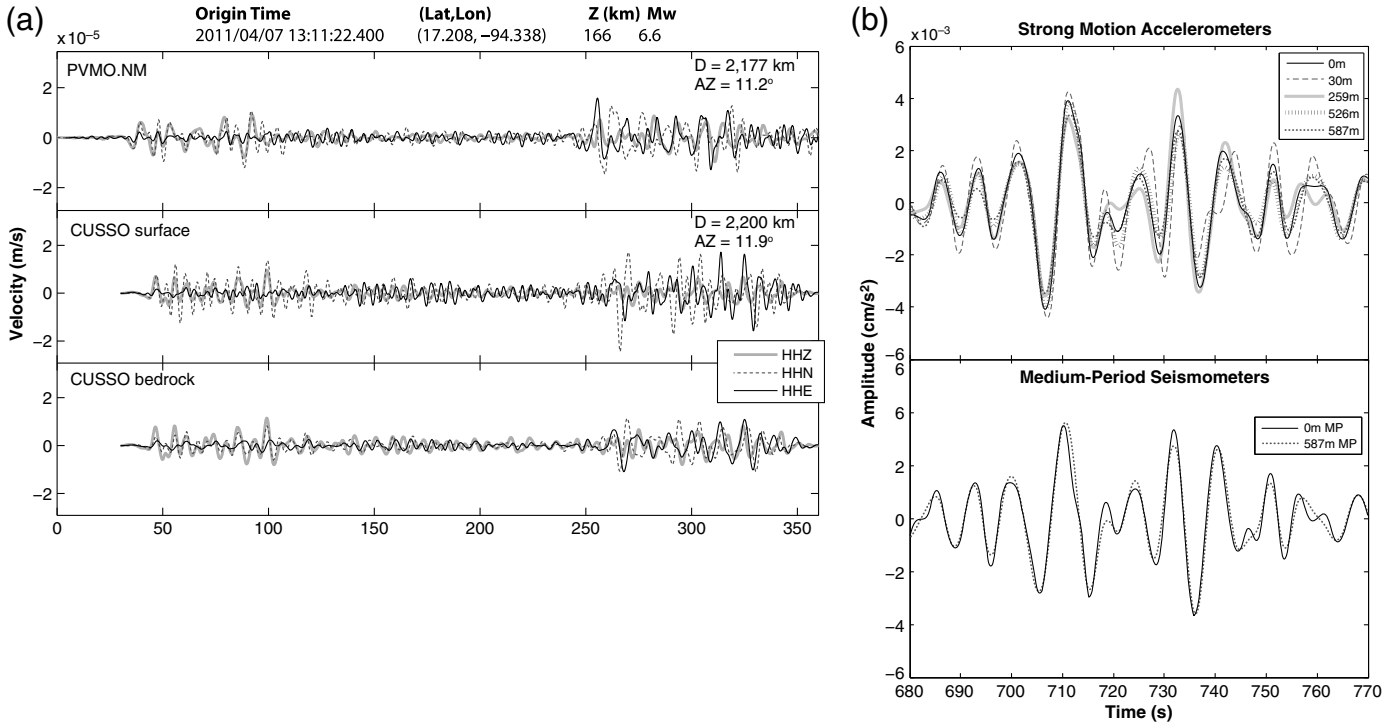

▲ **Figure 5.** (a) Vertical, north, and east seismograms from an M_w 6.6 teleseismic earthquake recorded by the calibrated station PVMO (New Madrid network, operated by Center for Earthquake Research and Information [CERI]; top) and CUSSO's surface (middle) and bedrock (bottom) seismometers. Data are band-pass filtered to within the passband of all sensors and to equalize amplification from the vertically ascending waves at CUSSO (0.07 and 0.2 Hz), and they are corrected for the effects of the instruments. The similarity in the amplitudes and waveforms, also observed at other nearby CERI stations, indicates that CUSSO's instrument responses are correct. (b) *S*-wave arrivals from the 9 March 2011 M_w 9.0 Tōhoku earthquake recorded on the (rotated) transverse components of CUSSO accelerometers (top) and seismometers (bottom), filtered from 0.07 to 0.2 Hz, with the effects of the instruments removed. The similarity in these waveforms recorded by the various instruments supports the accuracy of the instrument responses and the calculated sensor orientations.

bedrock interface (i.e., 587 m). An additional accelerometer was placed in the deep borehole at a depth of 526 m, just below the major velocity boundary that defines the top of the McNairy–Clayton formation (Figs. 3 and 4).

Instrumentation and Metadata

The instrumentation in descending elevation includes (1) an EENTEC SP-400 medium-period seismometer and Kinemetrics FBA-23 strong-motion accelerometer at the surface, (2) Kinemetrics HypoSensor (through 2 December 2010) or FBA-23 strong-motion accelerometer (after 2 December 2010) at 30 m, (3) Kinemetrics FBA-23 strong-motion accelerometer at 259 m, (4) EENTEC EA-120 strong-motion accelerometer at 526 m, and (5) EENTEC SP-400 medium-period seismometer and EENTEC EA-120 strong-motion accelerometer within the bedrock at 587 m. The medium-period seismometers have flat responses to ground velocity between 0.067 and 50 Hz. The Kinemetrics strong-motion accelerometers have full-scale acceleration thresholds between 0.25 and 1.0*g*, and the EENTEC EA-120 strong-motion accelerometers have a full-scale acceleration threshold of 2.0*g*. All of the strong-motion accelerometers have nominal corner frequencies of 50 Hz except the HypoSensor, which has a nominal corner frequency of 200 Hz. The 21 components are record by a Kinemetrics Granite datalogger. The system consists of 32 channels configured with unity gain and variable full-scale input voltages, 24-bit data, and an antialiasing filter. The antialiasing filter is a double-precision finite-impulse response acausal filter, attenuating the output by more than 140 dB at the Nyquist frequency.

The multiple installation cycles of the CUSSO borehole sensors were problematic, because these sensors lack internal compasses; thus, the orientations of their horizontal components were unknown and likely differed for each reinstallation. During the time period of the peak earthquake activity (from 20 December 2010 through 27 April 2011); however, all borehole-sensor orientations were estimated by cross-correlating long-period waveforms (i.e., periods greater than 4 s, which do not experience significant modification as they ascend the sediment column) from teleseismic earthquakes recorded by the borehole sensors' transverse components with the east-component recording at the surface (Brengman, 2014).

The metadata, including instrument responses, for the CUSSO array was assembled in dataless SEED format, incorporating vendor-supplied sensor calibrations (Brengman, 2014). The accuracies of the instrument responses were verified by comparing long-period observations from CUSSO with recordings from nearby calibrated stations (Fig. 5a) and then comparing CUSSO recordings of long-period phases at each component

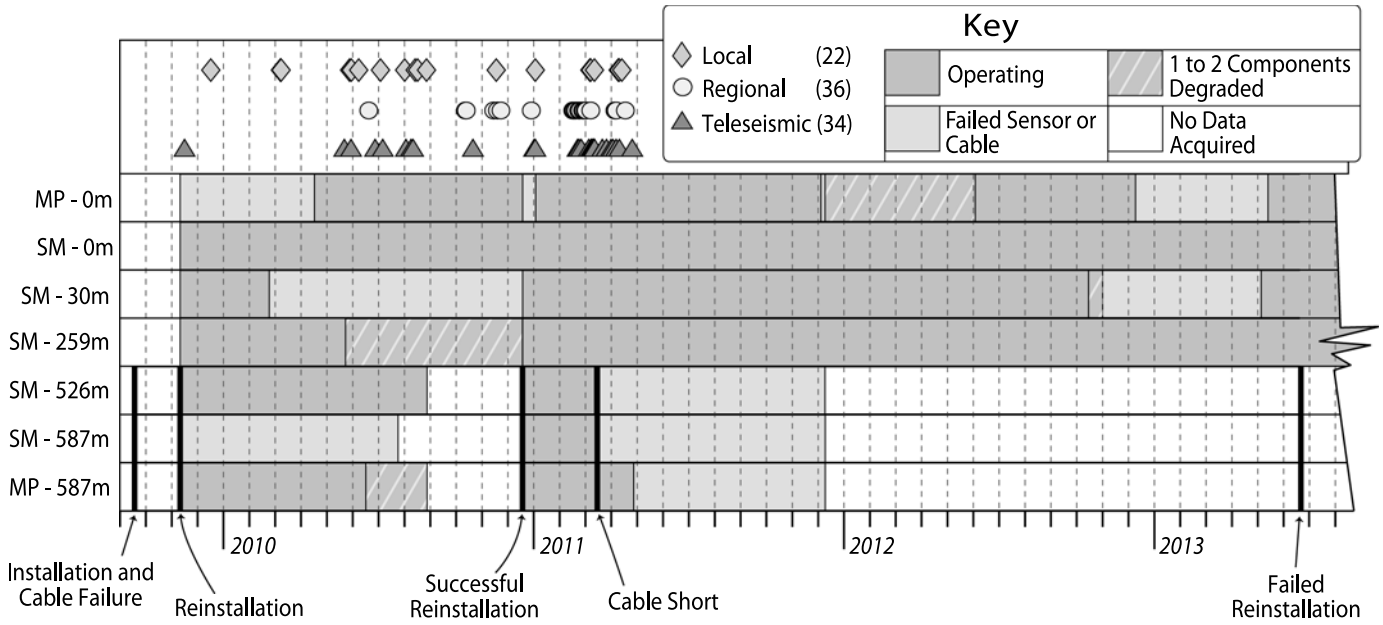

▲ **Figure 6.** Graphical summary of CUSSO's history, focusing on when the deepest-borehole sensors recorded earthquakes, including recorded earthquakes (top) and the operational status of each sensor during this time (lower grid): MP, medium-period seismometer; SM, strong-motion accelerometer. Events of significance in CUSSO's deep borehole are indicated with a heavy black line and are labeled. The time span also includes the most recent attempt at reinstallation in June 2013. The array status following the 2013 failed reinstallation continues through the present, as shown.

(Fig. 5b). Long-period waveforms (periods greater than 4 s) recorded in the vicinity of CUSSO experience limited-to-no amplification due to resonance and to the decreasing velocity up the sediment column. Also, at longer periods (wavelengths greater than four times the sediment thickness), sensors at all depths within the CUSSO array uniformly experience the effect of the free surface (Shearer and Orcutt, 1987).

Operational History

Operation of the full CUSSO array has been interrupted multiple times since its installation by either failure of a deep-hole sensor or their connectors (526 and 587 m sensors) and sheared cable from high hydrostatic pressures (~850 psi at 587 m). The sensors at the surface, 30 m, and 259 m also encountered occasional problems related to damage from lightning strikes and various mechanical problems. Figure 6 is a graphical summary of CUSSO's operational history, focusing on the period of time from the installation of the deep-hole sensors through the most recent reinstallation attempt and on the earthquakes it recorded while the deep-hole sensors were installed. The most recent attempt to reinstall the bedrock sensors was in June 2013; however, within a few hours of the installation signal interruption occurred due to a pressure-induced cable failure.

Originally, the datalogger at CUSSO was configured to operate in trigger mode only, recording all channels at 200 samples/s. Event triggering continues through the present; however, in October 2012, the University of Kentucky also began acquiring data from CUSSO in real time, and, in June 2013, the sample rate was reduced to 100 samples/s.

SEISMIC RECORDINGS AND ANALYSIS

Despite the instrumentation problems, the CUSSO array has recorded 95 earthquakes at local (24 earthquakes; offsets less than 130 km; magnitudes from 1.3 to 3.1), regional (37 earthquakes; offsets from 300 to 1550 km; magnitudes from 2.4 to 5.2), and teleseismic (34 earthquakes; offsets greater than ~20°; magnitudes from 5.0 to 9.0) distances (Fig. 7). We analyzed earthquake recordings acquired from November 2009 through April 2011, when, for all but approximately 3.5 months of that period, at least one of the bedrock sensors was operational (Fig. 6). Notably, the array recorded 33 earthquakes in the 2010–2011 Guy–Greenbrier earthquake swarm (Arkansas). We examined waveforms, amplitude spectra, and spectral ratios within the frequency band of engineering interest, specifically 0.1–20 Hz, which coincides with the frequency band of consistently useful data (i.e., instrument noise commonly dominates CUSSO's weak-motion accelerometer recordings for frequencies outside this band). However, no CUSSO records contain strong-ground motions; very few recorded amplitudes exceed 1 cm/s^2. The peak acceleration recorded to date was 1.8 cm/s^2 from a magnitude (M) 3.1 earthquake 22 km away. The numerous weak-motion recordings yielded high-quality observations, however.

Waveforms from the largest event in the Guy–Greenbrier earthquake sequence, an **M** 4.7 earthquake on 28 November

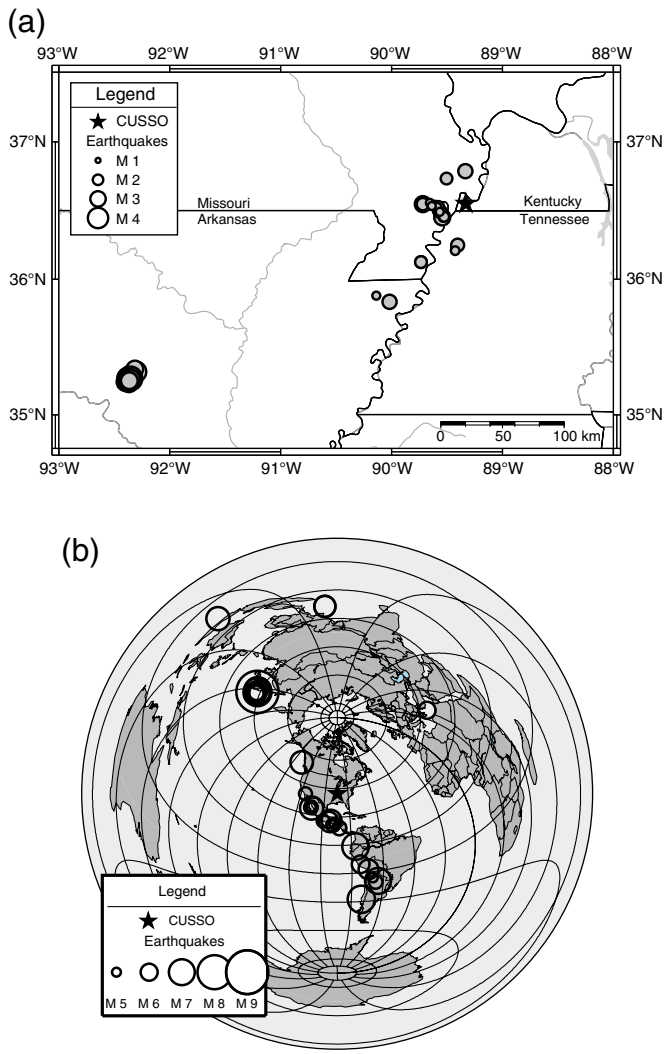

▲ **Figure 7.** (a) Local and regional and (b) teleseismic earthquake locations recorded from CUSSO's original installation through the April 2011 failure of sensors in the deep hole (526 and 587 m).

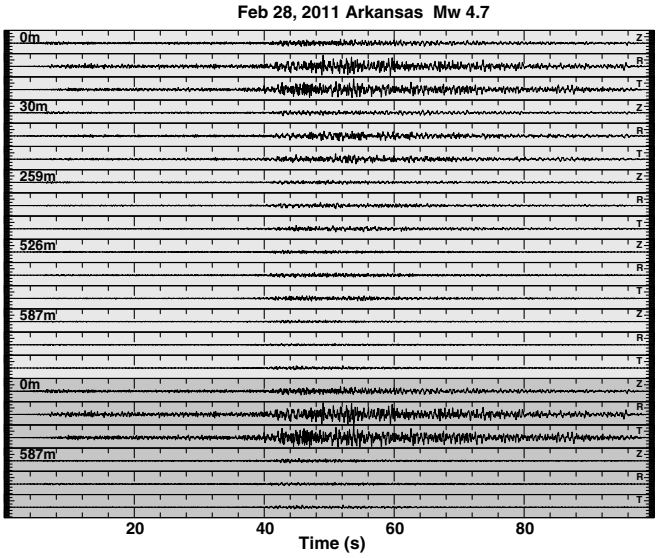

▲ **Figure 8.** Waveforms recorded on the full CUSSO array from the 28 February 2011 M 4.7 Arkansas earthquake, 308 km to the west-southwest. Traces are instrument corrected, the horizontal components rotated to radial and transverse orientations, and the data band-pass filtered from 0.5 to 12 Hz. All traces are scaled to the maximum amplitude of approximately 0.8 cm/s^2. Strong-motion accelerometer recordings have a light background, and seismometer recordings have a darker background.

2011, are shown in Figure 8 as an example of earthquake waveforms recorded by the full array. Although CUSSO was too far from this earthquake (308 km) to experience strong ground motion, the signal quality is good and exceeded the noise across our frequency band of interest (Fig. 9). Figure 10 shows vertical-component waveforms of *P*- and *S*-phase arrivals from the bedrock to the surface as another example: an **M** 2.3 earthquake 22 km west of CUSSO. Multiple *P* wave and *sP* (*S*-to-*P* converted phases at the sediment–bedrock interface) reflections (both upgoing and downgoing) are apparent in the waveforms.

Spectral ratios from the CUSSO recordings provide additional insight into seismic-wave propagation and modification through the sediment overburden. In Figure 11, we plot ratios of *S*-wave amplitude spectra (H/H) between each adjacent instrumented interval for three of the best-recorded (i.e., clearest signal) earthquakes, including the two with the largest ground motions, to estimate four transfer functions in the instrumented intervals between the bedrock and ground surface. The earthquakes, with a magnitude range between 2.7 and 4.7, occurred at back azimuths between 240° and 360° and at distances between 22 and 308 km. Horizontal-component amplitude spectra are calculated from the square root of the sum of the squares of the orthogonal horizontal components, and the ratios are smoothed with a running average using a 0.5 Hz Hanning window. The transfer functions generally are consistent between the events. Beginning with the deepest interval (i.e., McNairy–Clayton formation), there is a small amplification factor of approximately 1.5 between the bedrock and 526 m. The second interval, between 526 and 259 m, is comprised primarily of the Porters Creek clay and Wilcox formation. The amplitude response for this section is markedly frequency dependent; specifically, below ~2 Hz, there is an average amplification factor of approximately 2. However, amplification decreases above 2 Hz, and amplitudes are attenuated for frequencies above 7 Hz. The third interval, between 259 and 30 m, is primarily comprised of the Claiborne group and Jackson formation. Similar to the previous interval, amplitudes for these sediments are also amplified by a factor of ~2; however, two spectral peaks emerge at 1.1 and 3.2 Hz, suggesting resonance is established within the Claiborne–Jackson interval. The near-surface interval, between 30 m and the ground surface, is within the late Quaternary sediment. Frequencies are largely unamplified, or even attenuated, below 1 Hz; however, for frequencies above 1 Hz, a distinct frequency-dependent amplification occurs as manifested by three dominant spectral peaks at 2, 5.5, and 11 Hz. In addition, a general increase in

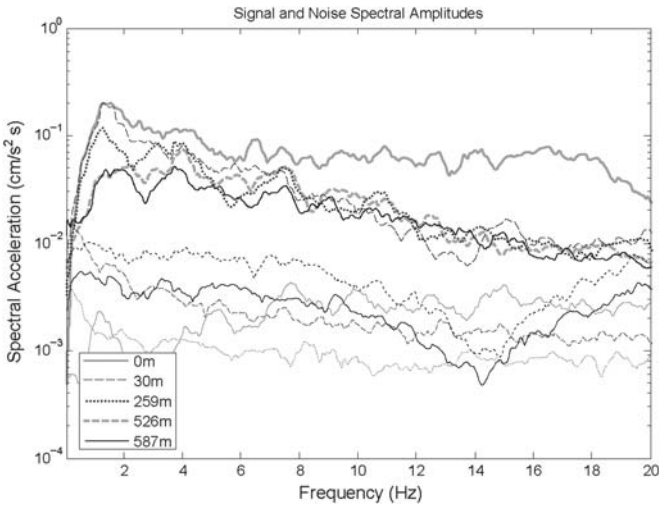

▲ **Figure 9.** Acceleration amplitude spectra of the vertical-component recordings of *P* and *S* waves from the 28 February 2011 magnitude 4.7 earthquake (upper bold lines) and preevent noise (lower thin lines). The plotted line styles are common between the signal and noise amplitude spectra. All spectra have been smoothed with a 1 Hz running average.

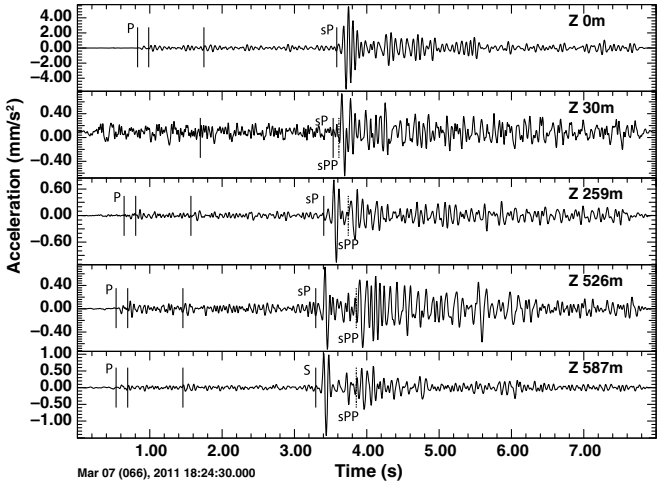

▲ **Figure 10.** Vertical-component recordings, scaled individually by trace, of an **M** 2.3 earthquake 22 km west of CUSSO. Waveforms are instrument-corrected and band-pass filtered from 3 to 20 Hz. *P* phase, *sP* (upgoing *S*-to-*P* conversion), and *sPP* (descending *sP* phase reflected from the free surface) arrivals are shown with a vertical line (dashed for *sPP* phase) and labeled with the corresponding phase. Other upgoing *P*-wave arrivals are indicated with unlabeled vertical lines. Additional up and downgoing *P* and *sP* reflections are less clear but extant in these waveforms.

response at frequencies above approximately 5 Hz is observed. The frequencies for the first two spectral peaks are consistent with the fundamental (1.8 Hz) and first-harmonic (5.4 Hz) frequencies estimated from the average shear-wave velocity between the ground surface and 30 m depth (Fig. 4). This interval in Figure 11 also illustrates the need for understanding the potential for noise to adversely affect a spectral ratio calculation. For example, the signal-to-noise ratio in these recordings is approximately 1 for the 30 and 259 m accelerometers across all frequencies; consequently, the increased low-frequency noise at 30 m relative to the surface observation results in an artificially low (i.e., noise suppression) H/H for the **M** 2.7 event at frequencies below 10 Hz.

We also determined H/V spectral ratios of the *S*-wave window for the same three earthquake surface recordings used in the H/H calculations (Fig. 12). A comparison of H/H and H/V indicates distinct low-frequency spectral peaks at approximately 0.3 and 0.8 Hz. These peaks are exhibited in each event with minor spectral shifts. The most notable shift in H/V response occurs for the M 4.7 event, which is lower than the other events; however, this lower peak more closely correlates to the theoretical fundamental frequency for the entire sediment column, including observed H/H results. Having said that, the frequencies at which all these peaks occur are generally consistent with the fundamental frequency (0.26 Hz) and first harmonic (0.78 Hz) estimated for the total overburden. However, we also find the average spectral ratios (i.e., amplification) are only coincident within a narrow band between 0.35 and 1.1 Hz: at lower frequencies (<0.35 Hz), H/V consistently exhibits larger amplification than H/H, whereas at higher frequencies (>1.1 Hz) H/H is consistently larger than H/V. The smallest earthquake (**M** 2.7) reduces the average H/H for frequencies less than 1.2 Hz but is consistent with the H/H of the larger earthquakes for higher frequencies. For all frequencies, there is greater variability in H/H than in H/V. Furthermore, the relatively narrow predominant response peak in the upper 30 m for both methods (~1.8 Hz) does not fully characterize the complete high-frequency amplification from the entire sediment column, which occurs over a much broader frequency range (up to ~7 Hz) for comparable and greater amplifications.

DISCUSSION AND CONCLUSIONS

The CUSSO installation has provided one of the few opportunities in the northern Mississippi embayment to geologically describe and geophysically measure the thick post-Paleozoic sediment. The installation's deepest borehole penetrated the entire 585-m-thick sediment overburden and terminated into the top of Late Ordovician limestone. The complex stratigraphy consists of Late Cretaceous through Holocene sands, clays, silts, and gravels, which are interpreted as a seven-layer intrasediment velocity model using data from downhole suspension velocity logs, surface seismic reflection and refraction surveys, and observed seismic wave propagation across the vertical seismic array. The *S*- and *P*-wave velocities for the sediment range between 160 and 875 m/s and between 1000 and 2300 m/s, respectively. The interpreted velocity model correlates well with those derived from local and regional seismic reflection and refraction surveys (Woolery and Wang, 2012; Woolery and Almayahi, 2014). Observed time differences for *S*- and *P*-wave propagation between the bedrock and surface sensors show bulk average velocities of 610 and 1836 m/s, respectively.

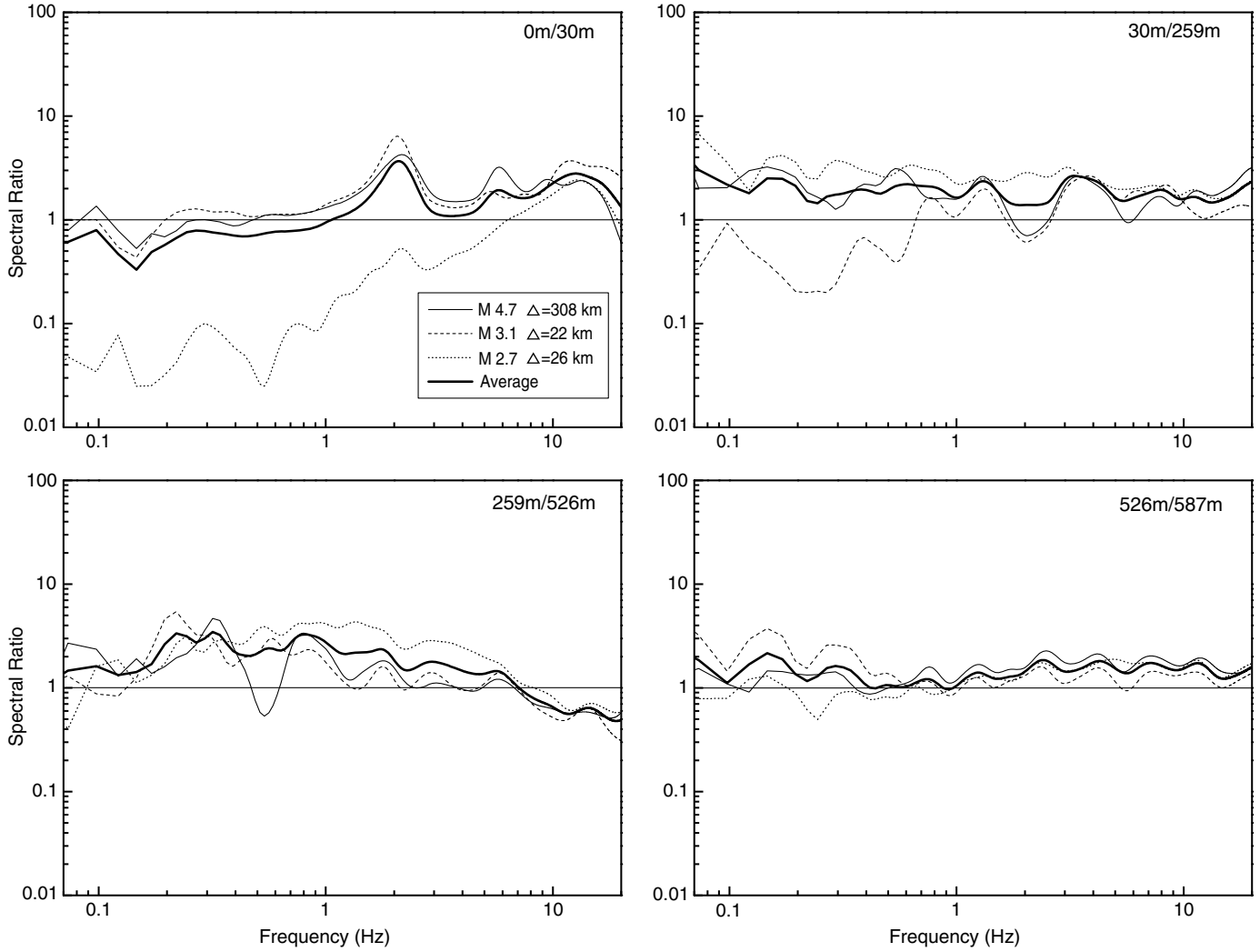

▲ **Figure 11.** Spectral ratios for three earthquakes at the four sequentially instrumented intervals of the vertical array. Ratios are calculated from acceleration amplitude spectra, smoothed with a 0.5 Hz Hanning window running average. The bold, solid line in each plot is the averaged spectral ratio from the three events. The ratios suggest earthquake motions are least affected by the 526-to-587 m interval but undergo a relatively broader spectral amplification and de-amplification in the 259-to-526 m interval, at frequencies below and above 7 Hz, respectively. Amplification is more uniform in the 30-to-259 m interval, with the appearance of weak spectral peaks, suggesting intrainterval resonance. Dominant response peaks, corresponding with the fundamental frequency and first-harmonic resonance in the upper 30 m, and overall higher frequency amplification is observed in the 0-to-30 m interval.

The *S*- and *P*-wave bedrock velocities measured by the suspension logs are 1452 and 3775 m/s, respectively. The site geology is complicated by a prominent northeast-oriented fault zone beneath the array and is interpreted as a Quaternary fault (see Woolery and Almayahi, 2014).

In terms of its primary engineering seismology objectives and despite operational difficulties, CUSSO has recorded high-quality earthquake waveforms that provide insight into seismic-wave propagation in the thick Mississippi embayment sediments, including alterations in the resultant waveform amplitude, frequency content, and duration. These alterations result from nonuniform transfer functions through the sediment overburden, with different frequencies being amplified or de-amplified in different intervals (Fig. 11). Although CUSSO has a limited dataset during the period with an operational bedrock sensor (or sensors), the initial observations from the various weak-motion responses indicate the site effect in this deep-sediment setting is not simply an effect of the shallowest layers; thus, characterization of the upper 30 m in thick sediments, such as found in the Mississippi embayment, may not be accurate for larger earthquakes (e.g., compare the 0 m/30 m in Fig. 11 with the average H/H and H/V curves in Fig. 12). These observations emphasize the concerns raised by previous studies considering V_{S30} as a sole means for site-effect evaluation (e.g. Chapman *et al.*, 2006; Castellaro *et al.*, 2008; among others). We also note that, in our preliminary H/V measurements, the vertical and horizontal bedrock amplitudes are not equal (i.e., the average ratio in bedrock is consistently greater

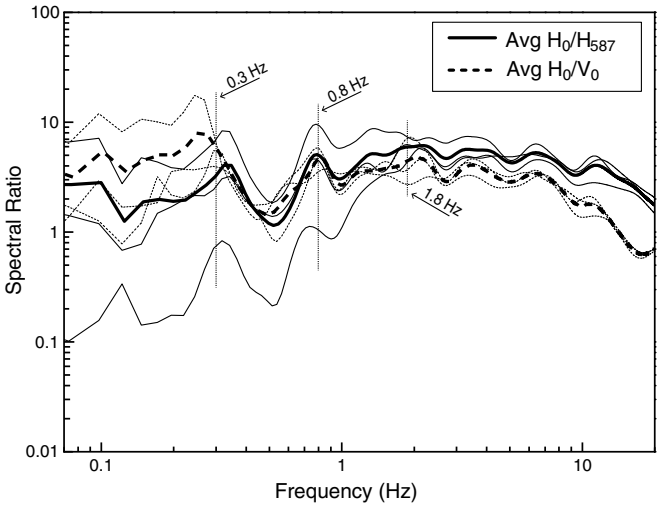

▲ **Figure 12.** Average surface-to-bedrock spectral ratio (bold, solid line) and average horizontal-to-vertical (H/V) spectral ratio at the surface (bold, dashed line), averaged from three earthquakes (solid and dashed thin lines, respectively). Ratios are calculated from acceleration amplitude spectra, smoothed with a 0.25 Hz window-length running average. There are notable low-frequency spectral peaks consistently at approximately 0.3 and 0.8 Hz. The frequencies at which these peaks occur are consistent with the fundamental frequency (0.26 Hz) and the first harmonic (0.78 Hz) estimated for the entire sediment column. However, the average spectral ratios are only coincident within a narrow band between 0.35 and 1.1 Hz: at lower frequencies (<0.35 Hz), H/V consistently indicates greater amplification than H/H, whereas at higher frequencies (>1.1 Hz), H/H is consistently larger than H/V. The predominant peak in the upper 30 m response (1.8 Hz; Fig. 11) does not characterize the broader range of frequencies that experience comparable or greater levels of amplification.

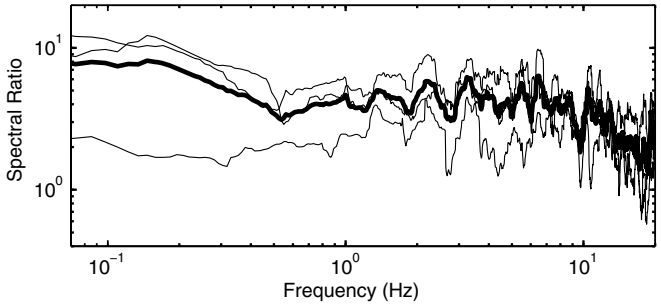

▲ **Figure 13.** H/V spectral ratios of the bedrock seismometer recordings for the three earthquakes used in Figures 11 and 12 (thin lines) and their average (thick line). Ratios are calculated from acceleration amplitude spectra and smoothed with a 0.5 Hz window-length running average. With the exception of frequencies higher than 15 Hz, horizontal amplitudes are consistently greater than vertical amplitudes.

than unity); an assumption that is required for applying this method to site characterization (Fig. 13). We speculate this may be due to the deep weathering and fracturing at the large unconformity separating the Cretaceous sediment and Ordovician limestone; however, additional data are needed to confirm the initial observations. Further, there are noticeable differences between the spectral ratios from the directly measured transfer function (H/H) and that estimated by H/V (e.g., Fig. 12): the two are consistent only for a narrow band of frequencies. The effectiveness of the H/V method has been evaluated by other experiments involving vertical seismic arrays, with variable results (e.g., Theodulidis *et al.*, 1996; Tsuboi *et al.*, 2001; Bonilla *et al.*, 2002). One contributor to the difference is the free surface, which only affects the bedrock-surface H/H spectral ratios at high frequency; H/V is insensitive to this effect because it is measured only at the surface, and the free-surface effect, experienced equally on all components, is removed by the ratio. Despite the differences, however, both methods reveal peaks in the response at approximately 0.3 and 0.8 Hz due to shear-wave resonance within the CUSSO sediment column.

Upgoing and downgoing phase arrivals (Fig. 10) will allow basic exploration of resonance, pulse modification (e.g., broadening), and evaluation of site velocity structure determined by various methodologies; however, operational stability of the full array is required for recording more earthquakes, particularly the infrequent strong-motion events, to thoroughly investigate these topics. Observations across a broader range of magnitudes (source effects) and epicentral distances and bearings (path effects) will provide a larger set of amplitude spectra and spectral ratios from the sensors at the different depths, thus providing statistically significant constraint for the various methodologies quantifying the site effect, as well as robust calibration for the free-field seismic stations in the regional networks. To do this, CUSSO will be upgraded with instrumental hardware that is more environmentally resilient to the existing elevated hydrostatic conditions. In addition, the EENTEC accelerometers deployed during the time of this study have been found to exhibit a hysteresis response for weak, long-period signals (Greg Steiner, personal comm., 2014). Although outside the range of engineering interest, this behavior results in a nonlinear and unpredictable response to low-level, long-period excitations and diminishes the data's usefulness for complete seismological applications. Nevertheless, the existing CUSSO data are useful for most purposes and are available for interested researchers; however, care must be taken to avoid incorporating undesirable noise, including degraded signal from a failing component, in any analysis by referring to the graphical history in Figure 6 as a guide for earthquake record selection during periods when sensors at the desired depths were properly operating.

DATA AND RESOURCES

All data presented in this study are part of the Kentucky Seismic and Strong Motion Network database. Instrument response compilation and response plots were made at the University of Kentucky with Incorporated Research Institutions for Seismology (IRIS) software. All data are available for

download from http://kgs.uky.edu/kgsweb/main.asp (last accessed April 2015).

ACKNOWLEDGMENTS

This work was financially supported by U.S. Geological Survey–National Earthquake Hazards Reduction Program (NEHRP) (Awards 08HQGR0094 and G11AP20156), Department of Energy/Kentucky Research Consortium for Energy and Environment (Award DE-FG05-03OR23032), and the Kentucky Geological Survey (KGS). The authors appreciate Jonathan McIntyre (deceased) for his effort in drilling the deepest borehole and initial instrument installation. We also appreciate Steve Martin and Steve Greg for their help with the stratigraphy interpretation, as well as Daniel Hunter, Shoba (Gowda) Dickinson, Anthony Paschall, David Butler, Carrington Wright, and Ali Almayahi, who provided essential data acquisition and processing assistance. We also thank Mianshui Rong for his processing assistance, as well as Terry Hounchell and Collie Rulo (KGS) for their graphic arts support. Martin Chapman and Randy Cox, as well as an anonymous reviewer improved the article considerably with their insightful comments and suggestions.

REFERENCES

Anderson, J. G., Y. Lee, Y. Zeng, and S. Day (1996). Control of strong motion by the upper 30 meters, *Bull. Seismol. Soc. Am.* **86,** 1749–1759.

Archuleta, R. J., S. H. Seale, P. V. Sangas, L. M. Baker, and S. T. Swain (1992). Garner Valley downhole array of accelerometers: Instrumentation and preliminary data analysis, *Bull. Seismol. Soc. Am.* **82,** 1592–1621.

Bard, P.-Y., and F. J. Chavez-Garcia (1993). On the decoupling of surficial sediments from surrounding geology at Mexico City, *Bull. Seismol. Soc. Am.* **83,** 1979–1991.

Bodin, P., and S. Horton (1999). Broadband microtremor observation of basin resonance in the Mississippi embayment, central US, *Geophys. Res. Lett.* **26,** 903–906.

Bommer, J. J., and N. A. Abrahamson (2006). Why do modern probabilistic seismic-hazard analyses often lead to increased hazards estimates? *Bull. Seismol. Soc. Am.* **96,** 1967–1977.

Bonilla, L. F., J. H. Steidl, G. T. Lindley, J.-C. Gariel, and R. J. Archuleta (2002). Borehole response studies at the Garner Valley downhole array, southern California, *Bull. Seismol. Soc. Am.* **92,** 3165–3179.

Bonilla, M. G. (1991). The Marina District, San Francisco, California: Geology, history, and earthquake effects, *Bull. Seismol. Soc. Am.* **81,** 1958–1979.

Bonnefoy-Claudet, S., F. Cotton, and P.-Y. Bard (2006). The nature of noise wavefield and its applications for site effect studies: A literature review, *Earth Sci. Rev.* **79,** 205–227.

Brengman, C. (2014). Instrument correction and dynamic site profile validation at the Central United States Seismic Observatory, New Madrid seismic zone, *Master's Thesis*, University of Kentucky, Lexington, Kentucky, 284 pp.

Building Seismic Safety Council (2009). National Earthquake Hazards Reduction Program Recommended Provisions and Commentary for Seismic Regulations for New Buildings and Other Structures (FEMA P-750/2009 Edition): Part I (Provisions) and Part II (Commentary), Federal Emergency Management Agency, Washington, D.C., 6–8.

Castallero, S., and F. Mulargia (2009). The effect of velocity inversions on H/V, *Pure Appl. Geophys.* **166,** 567–592.

Castellaro, S., F. Mulargia, and P. L. Rossi (2008). V_{S30}: Proxy for seismic amplification? *Seismol. Res. Lett.* **79,** 540–543.

Castro, R. R., M. Mucciarelli, F. Pacor, and C. Petrungaro (1997). *S*-wave site-response estimates using horizontal-to-vertical spectral ratios, *Bull. Seismol. Soc. Am.* **87,** 256–260.

Chapman, M. C., J. R. Martin, C. G. Olgun, and J. N. Beale (2006). Site-response models for Charleston, South Carolina, and vicinity developed from shallow geotechnical investigations, *Bull. Seismol. Soc. Am.* **96,** 467–489.

Chen, S.-Z., and G. M. Atkinson (2002). Global comparisons of earthquake source spectra, *Bull. Seismol. Soc. Am.* **92,** 885–895.

Cox, R. T., and R. B. Van Arsdale (2002). The Mississippi embayment, North America: A first order continental structure generated by the Cretaceous superplume mantle event, *J. Geodyn.* **34,** 163–176.

Csontos, R., and R. Van Arsdale (2008). New Madrid seismic zone fault geometry, *Geosphere* **4,** 802–813.

Davis, R. W., T. W. Lambert, and A. J. Hansen Jr. (1973). Subsurface geology and ground-water resources of the Jackson Purchase region, Kentucky, *U.S. Geol. Surv. Water-Supply Paper 1987*, 66 pp.

Field, E. H., S. Kramer, A.-W. Elgamal, J. D. Bray, N. Matasovic, P. A. Johnson, C. Cramer, C. Roblee, D. J. Wald, L. F. Bonilla, *et al.* (1998). Nonlinear site response: Where we're at (a report from a SCEE/PEER seminar and workshop), *Seismol. Res. Lett.* **69,** 230–234.

Finch, W. I. (1971). Geologic map of the Bondurant quadrangle, Fulton County, Kentucky, and New Madrid, Mississippi County, Missouri, *U.S. Geological Survey*, 7.5-minute geological quadrangle, GQ 918, 1:24,000 scale, one sheet.

Horton, S. (2012). Disposal of hydrofracking waste fluid by injection into subsurface aquifers triggers earthquake swarm in central Arkansas with potential of damaging earthquake, *Seismol. Res. Lett.* **83,** 250–260.

Johnston, A. C., and E. S. Schweig (1996). The enigma of the New Madrid earthquakes of 1811–1812, *Annu. Rev. Earth Planet. Sci.* **24,** 339–384.

Lermo, J., and F. J. Chavez-Garcia (1993). Site effect evaluation using spectral ratios with only one station, *Bull. Seismol. Soc. Am.* **83,** 1574–1594.

McDowell, R. C., G. J. Grabowski, and S. L. Moore (1981). Geologic map of Kentucky, *U.S. Geological Survey*, 1:250,000 scale, three sheets.

Molnar, S., J. F. Cassidy, and S. E. Dosso (2004). Comparing intensity variation of the 2001 Nisqually earthquake with geology in Victoria, British Columbia, *Bull. Seismol. Soc. Am.* **94,** 2229–2238.

Nakamura, Y. (1989). A method for dynamic characteristics estimation of subsurface using microtremor on the ground surface, *Q. Rep. Railway Tech. Res. Inst.* **30,** 25–33.

Nelson, W. J. (1998). Bedrock geology of the Paducah 1° × 2° CUSMAP quadrangle, Illinois, Indiana, Kentucky, and Missouri, *U.S. Geol. Surv. Bull.* **2150-B,** 36 pp.

Olive, W. W. (1980). Geologic maps of the Jackson Purchase region, Kentucky, *U.S. Geol. Surv. Misc. Invest. No. I-1217*, 1 sheet, and 11 page pamphlet.

Potter, P. E., and W. A. Pryor (1961). Dispersal centers of Paleozoic and later clastics of the upper Mississippi Valley and adjacent areas, *Geol. Soc. Am. Bull.* **72,** 1195–1250.

Schwalb, H. R. (1969). Paleozoic geology of the Jackson Purchase region, Kentucky, *Report of Investigations (Kentucky Geological Survey)*, series 10, 40 pp.

Seed, H. B., M. P. Romo, J. I. Sun, A. Jaime, and J. Lysmer (1988). The Mexico earthquake of September 19, 1985–Relationships between soil conditions and earthquake ground motions, *Earthq. Spectra* **4,** 687–729.

Shearer, P. M., and J. A. Orcutt (1987). Surface and near-surface effects on seismic waves—Theory and borehole seismometer results, *Bull. Seismol. Soc. Am.* **77,** 1168–1196.

Steidl, J. H., A. G. Tumarkin, and R. J. Archuleta (1996). What is a reference site? *Bull. Seismol. Soc. Am.* **86,** 1733–1748.
Theodulidis, N., P.-Y. Bard, R. Archuleta, and M. Bouchon (1996). Horizontal-to-vertical spectral ratio and geological conditions: The case of Garner Valley downhole array in southern California, *Bull. Seismol. Soc. Am.* **86,** 306–319.
Toro, G. R., W. J. Silva, R. K. McGuire, and R. B. Herrmann (1992). Probabilistic seismic hazard mapping of the Mississippi embayment, *Seismol. Res. Lett.* **63,** 449–475.
Tsuboi, S., M. Saito, and Y. Ishihara (2001). Verification of horizontal-to-vertical spectral-ratio technique for estimation of site response using borehole seismographs, *Bull. Seismol. Soc. Am.* **91,** 499–510.
Tuttle, M. P., E. S. Schweig, J. D. Sims, R. H. Lafferty, L. W. Wolf, and M. L. Haynes (2002). The earthquake potential of the New Madrid seismic zone, *Bull. Seismol. Soc. Am.* **92,** 2080–2089.
Van Arsdale, R. B., and R. K. TenBrink (2000). Late Cretaceous and Cenozoic geology of the New Madrid seismic zone, *Bull. Seismol. Soc. Am.* **90,** 345–356.
Wald, L. A., and J. Mori (2000). Evaluation of methods for estimating linear site-response amplifications in the Los Angeles region, *Bull. Seismol. Soc. Am.* **90,** no. 6B, S32–S42.
Woolery, E., and A. Almayahi (2014). Northeast-oriented transpression structure in the northern New Madrid seismic zone—Extension of a shear zone across the Reelfoot fault stepover arm, *Bull. Seismol. Soc. Am.* **104,** 2587–2596.
Woolery, E., and Z. Wang (2010). Toward construction of the Central United States Seismic Observatory and Calibration Site: Defining the geologic site model, *U.S. Geol. Surv. National Earthquake Hazards Reduction Program Final Technical Rept. 08HQGR0094*, 33 pp.
Woolery, E., and Z. Wang (2012). Toward construction of the Central United States Seismic Observatory and Calibration Site: Defining the geologic site model part 2, *U.S. Geol. Surv. National Earthquake Hazards Reduction Program Final Technical Rept. G11AP20156*, 32 pp.

Edward W. Woolery[1]
Clayton Brengman
Department of Earth and Environmental Sciences
University of Kentucky
Lexington, Kentucky 40506 U.S.A.
ewoolery@uky.edu

Zhenming Wang
N. Seth Carpenter[2]
Kentucky Geological Survey
University of Kentucky
Lexington, Kentucky 40506 U.S.A.

Ron Street
University of Kentucky (emeritus)
13813 Werth Road
Hermosa, South Dakota 57744 U.S.A.

Published Online 16 December 2015

[1] Also at Kentucky Geological Survey, University of Kentucky, Lexington, Kentucky 40506 U.S.A.
[2] Also at Department of Earth and Environmental Sciences, University of Kentucky, Lexington, Kentucky 40506 U.S.A.